

AD-763 120

THIN FILM OPTICAL WAVEGUIDES IN III-V
SEMICONDUCTORS

M. George Craford

Monsanto Company

Prepared for :

Air Force Cambridge Research Laboratories

January 1973

DISTRIBUTED BY:

NTIS

National Technical Information Service
U. S. DEPARTMENT OF COMMERCE
5285 Port Royal Road, Springfield Va. 22151

AD 763120

THIN FILM OPTICAL WAVEGUIDES
IN
III-V SEMICONDUCTORS



by

M. George Craford

Monsanto Company
Electronic Products Division
800 N. Lindbergh Boulevard
St. Louis, Missouri 63166

Contract No. F19628-72-C-0324
Project No. 2074

Semi-Annual Technical Report

January 1973

Contract Monitor: Andrew C. Yang
Solid State Sciences Laboratory

Reproduced by
NATIONAL TECHNICAL
INFORMATION SERVICE
U.S. Department of Commerce
Springfield, VA 22151

Approved for public release; distribution unlimited.

Sponsored by
Defense Advanced Research Projects Agency
ARPA Order No. 2074

Monitored by
AIR FORCE CAMBRIDGE RESEARCH LABORATORIES
AIR FORCE SYSTEMS COMMAND
UNITED STATES AIR FORCE
BEDFORD, MASSACHUSETTS 01730

Unclassified

Security Classification

DOCUMENT CONTROL DATA - R & D

(Security classification of title, body of abstract and indexing annotation must be entered when the overall report is classified)

1. ORIGINATING ACTIVITY (Corporate author) Monsanto Company 800 N. Lindbergh Blvd. St. Louis, Missouri 63166		2a. REPORT SECURITY CLASSIFICATION Unclassified	
		2b. GROUP	
3. REPORT TITLE THIN FILM OPTICAL WAVEGUIDES IN III-V SEMICONDUCTORS			
4. DESCRIPTIVE NOTES (Type of report and inclusive dates) "Scientific. Interim".			
5. AUTHOR(S) (First name, middle initial, last name) M. George Craford			
6. REPORT DATE January, 1973		7a. TOTAL NO. OF PAGES 46	7b. NO. OF REFS 6
8a. CONTRACT OR GRANT NO. ARPA Order No. 2074 F19628-72-C-0324		8b. ORIGINATOR'S REPORT NUMBER(S) Semi-Annual Technical Report	
8c. PROJECT NO: Task, Work Unit Nos. 2074 n/a n/a		8d. OTHER REPORT NO(S) (Any other numbers that may be assigned (his report) AFCRL-TR 73-0197	
8d. DoD Element 61101E			
8d. DoD Subelement n/a			
10. DISTRIBUTION STATEMENT A - Approved for public release, distribution unlimited. studied on microfiche.			
11. SUPPLEMENTARY NOTES This research was sponsored by the Defense Advanced Research Projects Agency.		12. SPONSORING MILITARY ACTIVITY Air Force Cambridge Research Laboratories (LQ) L. G. Hanscom Field Bedford, Massachusetts 01730	
13. ABSTRACT The development of techniques for the growth of large area vapor phase epitaxial GaAs and GaAsP, and liquid phase epitaxial GaAs and GaAlAs, waveguide structures is described. The development of evaluation techniques for determining the attenuation rate in the waveguide structures is also discussed. Evaluation results obtained on an initial series of GaAs waveguide structures are described and compared to calculated attenuation rates			

DD FORM 1473

REPLACES DD FORM 1473, 1 JAN 64, WHICH IS OBSOLETE FOR ARMY USE.

Unclassified

Security Classification

Unclassified

Security Classification

14. KEY WORDS	LINK A		LINK B		LINK C	
	ROLE	WT	ROLE	WT	ROLE	WT
Gallium arsenide Gallium arsenide phosphide Gallium aluminum arsenide Vapor phase epitaxy Liquid phase epitaxy Integrated optics Thin film waveguides Electro-optical modulation Optical attenuation						

i-a

Security Classification

ABSTRACT

The development of techniques for the growth of large area vapor phase epitaxial GaAs and GaAsP, and liquid phase epitaxial GaAs and GaAlAs, waveguide structures is described. The development of evaluation techniques for determining the attenuation rate in the waveguide structures is also discussed. Evaluation results obtained on an initial series of GaAs waveguide structures are described and compared to calculated attenuation rates.

FOREWORD

This semi-annual technical report covers the work performed under contract F19628-72-C-0324 between the period July 1, 1972 to December 31, 1972.

The objective of this program is to grow a variety of epitaxial GaAs, GaAsP and GaAlAs waveguide structures and to evaluate their performance with regard to the propagation of 10.6 μm radiation. The effect of such parameters as layer thickness, alloy composition profile, and carrier concentration will be investigated. Vapor phase epitaxial techniques will be employed to grow the GaAsP structures and liquid phase epitaxial techniques to grow the GaAlAs structures.

Technical direction is being provided by Dr. Andrew Yang of the Air Force Cambridge Research Laboratory. The growth of the epitaxial structures is being carried out in the Monsanto Commercial Products Company, Electronic Products Division, Laboratories, St. Louis, Missouri, and the waveguide evaluation has been subcontracted to and is being performed in the laboratories of the Washington University School of Engineering and Applied Science, St. Louis, Missouri.

The research carried out on this program is under the direction of M. George Craford. Others directly involved in this work and in the preparation of this report are D. Finn, W. O. Groves, and A. H. Herzog, of Monsanto Company, and W. S. C. Chang, M. Muller, and H. R. Vann, of Washington University.

TABLE OF CONTENTS

	<u>Page No.</u>
I. SUMMARY OF RESULTS	1
A. VAPOR PHASE EPITAXY (VPE)	1
B. LIQUID PHASE EPITAXY (LPE)	1
C. WAVEGUIDE EVALUATION	1
II. VAPOR PHASE EPITAXY	2
A. INTRODUCTION	2
B. RESULTS OBTAINED IN PRODUCTION SCALE VPE REACTORS	2
C. RESULTS OBTAINED ON THE GROWTH OF HIGH RESISTIVITY GaAs IN RESEARCH SCALE REACTORS	4
D. WAVEGUIDE STRUCTURES SUBMITTED FOR EVALUATION	5
E. CONCLUSIONS	5
III. LIQUID PHASE EPITAXY	9
A. INTRODUCTION	9
B. EXPERIMENTAL SYSTEMS	9
1. Radiant Furnace LPE System	9
2. Resistance Furnace LPE System	12
C. EXPERIMENTAL RESULTS	12
1. Radiant Furnace System	12
2. Resistance Furnace System	14
D. CONCLUSIONS	14

TABLE OF CONTENTS (Continued)

	<u>Page No.</u>
IV. WAVEGUIDE EVALUATION	15
A. EXPERIMENTAL MEASUREMENT OF THE WAVEGUIDE ATTENUATION	15
1. Methods of Experimental Measurement	15
2. Experimental Data	22
B. THEORETICAL CALCULATIONS OF THE EFFECT OF SUBSTRATE CONDUCTIVITY ON WAVEGUIDE ATTENUATION	30
C. THEORETICAL ANALYSIS OF THE WAVEGUIDES WITH GRADED REFRACTIVE INDEX	32
D. DEVICE EXPERIMENTATION	33
1. Electro-Optical Modulation in Uniform Thin Film Waveguides	33
2. Experimentation with Two-Dimensional Waveguides	34
E. CONCLUSIONS	34
V. WORK FOR NEXT PERIOD	38
A. VAPOR PHASE EPITAXY	38
B. LIQUID PHASE EPITAXY	38
C. WAVEGUIDE EVALUATION	38
REFERENCES	39

LIST OF FIGURES

<u>FIGURE</u>		<u>Page No.</u>
1	Research Scale LPE Graphite Boat	10
2	Schematic Diagram of Gas Handling System	11
3	Schematic Diagram of Graphite Sliding-Boat System	13
4	Schematic Illustration of Attenuation Rate Measurement	16
5	The Prism-Prism Coupler Assembly	18
6	Measurements of Attenuation Rate by the Prism-Prism Coupler	19
7	The Experimental Setup for the Waveguide Evaluation	20
8	Schematic Diagram of the CO ₂ Laser Stabilizer	21
9	Photograph of the GaAs Epi-Layer Wafers	23
10	Calculated Curves for β/k_0 versus Film Thickness for Various Modes ($N_{\text{substrate}} = 1 \times 10^{17} \text{ cm}^{-3}$)	24
11	Calculated Curves for β/k_0 versus Film Thickness for Various Modes ($N_{\text{substrate}} = 6 \times 10^{17} \text{ cm}^{-3}$)	25
12	Calculated Curves for β/k_0 versus Film Thickness for Various Modes ($N_{\text{substrate}} = 1 \times 10^{18} \text{ cm}^{-3}$)	26
13	Calculated Curves for β/k_0 versus Film Thickness for Various Modes ($N_{\text{substrate}} = 4 \times 10^{18} \text{ cm}^{-3}$)	27
14	Relative Output Power as a Function of Path Length	28
15	Calculated Attenuation Rate due to Substrate Absorption	31
16	Schematic Illustration of Grating Electro-Optical Mode Conversion Modulator	35
17	Two Dimensional Electro-Optical Phase Modulator	36

LIST OF TABLES

<u>TABLE</u>		<u>Page No.</u>
I	Epitaxial GaAs Film Thickness Uniformity Using a Rotating Disk Holder	6
II	Emission Spectroscopy Analysis of Undoped Epi GaAs	7
III	Characteristics of GaAs/GaAs Waveguide Structures	8

SECTION I

SUMMARY OF RESULTS

The results of the activities during the first six months are summarized as follows:

A. VAPOR PHASE EPITAXY (VPE)

A modified reactor design has been developed which yields large area wafer with a film thickness uniformity of $\pm 5\%$.

A series of eight waveguide structures, consisting of a high resistivity GaAs epitaxial film on a low resistivity GaAs substrate have been grown and submitted for evaluation. The majority of waveguides submitted have useful lengths of ~ 2 inches.

An exploratory research program has been initiated in an attempt to grow high resistivity VPE epitaxial films ($\rho \gtrsim 10^6 \Omega\text{-cm}$), which would allow high duty cycle modulation of thin film GaAs waveguides.

B. LIQUID PHASE EPITAXY (LPE)

A reactor has been designed and constructed which should facilitate the growth of large area GaAlAs LPE epitaxial structures with uniform film properties.

C. WAVEGUIDE EVALUATION

A reliable method for the measurement of waveguide attenuation has been developed.

Significant experimental data and numerical results have been collected on high resistivity GaAs grown on low resistivity GaAs waveguides indicating the usefulness as well as the limitation of this type of waveguide.

An analysis of a waveguide with a graded refractive index has been made in preparation for future experimentation.

An initial experiment on electro-optical modulation has been designed and is in the process of being carried out.

SECTION II

VAPOR PHASE EPITAXY

A. INTRODUCTION

The objectives of the Vapor Phase Epitaxy portion of this program are to grow a variety of GaAs, GaAs/GaAsP, and GaAsP/GaAs/GaAsP, structures on GaAs substrates in order to determine the effect of carrier concentration, alloy composition, and layer thickness on waveguide properties at $10.6 \mu\text{m}$. During the first portion of this program only GaAs structures were grown.

B. RESULTS OBTAINED IN PRODUCTION SCALE VPE REACTORS

Experimental work for this program utilized a vertical flow, laminar type reactor called the Monsanto Mark II. Details of construction of the reactor except for two minor modifications and some dimensional changes are given in reference 1. The bottom section of the reactor incorporating the mixing and deposition zones was enlarged to 100 mm O.D. to accommodate crystals up to 8.5 cm in length. The quartz joint on top of the reactor was eliminated and the bottom was converted to a flange type vacuum o-ring seal to facilitate loading and unloading the reactor.

Epitaxial films grown for this program must be of high homogeneity and surface perfection and have uniform film thickness along the maximum crystal dimension. At the beginning of this work it was realized that film thickness uniformity could be a problem particularly in films 50 - 100 μm thick on large crystals. Variations in film thickness in the Mark II production reactors using an off-vertical type substrate holder, i.e., the wafer slightly inclined to the direction of gas flow, are typically $\pm 25\%$ in the axial direction and $\pm 10\%$ tangential to the base for crystals 2 inches in length. Hence, one apparent experimental problem is the control of the overall reaction rate in a system in which both the surface reaction and gas phase diffusion are significant and variable in the direction of gas flow. To circumvent problems of trying to compensate for directional changes in these two rates a rotating flat disk substrate holder (perpendicular to the gas flow) was investigated for film thickness uniformity. In laminar flow the important feature of the rotating disk is the independence of the concentration profile and diffusional resistance on radial position which should consequently ensure a uniform reaction rate over the surface of the disk. This is not the case with flow over a flat plate, for example, in which the surface reaction rate at constant temperature would decrease with distance from the leading flow edge.

Evaluation of the new type substrate holder was made with two substrates (approximately one inch in length) in each run placed at different radial positions on the disk. After deposition the wafers were cleaved along the major

dimension, stained and the film thickness measured microscopically. The results of the measurements on two different runs are given in Table I. The variation in film thickness, not counting edge crown effects or off-orientation flats, did not exceed ± 5 per cent within or between wafers.

Several problems have arisen with the deposition of GaAs films. The initial reactor installation produced undoped material of high resistivity ($\rho \approx 1 \times 10^{16}$ ohm-cm) with poor surface quality. The films were extremely hazy and contained a large number of deep pits. After 15 runs in which the growth parameters were changed to alleviate these conditions a pinhole leak was discovered in the quartz reactor. Another reactor was installed and immediately the surface quality improved. Additional adjustments in the growth conditions produced surfaces which contained only minor pit imperfections. These pits are shallow and have irregular shapes indicating a non crystallographic type origin. For example, defects of this type can occur if dust or other particulate matter is present or falls on the substrate during growth. Several runs were made with the production type holder previously described to investigate the feasibility of the problem being holder oriented. The same type pits occurred with the vertical holder and they were of approximately the same density. Whether or not these imperfections are a serious problem in the fabrication of waveguides will be determined during the course of this program.

Following substantial improvements in the surface quality of the films the system became highly contaminated giving undoped material of $1 \times 10^{18}/\text{cm}^3$ net carriers. Approximately two weeks were lost in locating the contamination source. The problem consisted of a contaminated AsH_3 supply and a leaking dopant valve, the latter contributing most of the trouble. All of the feed system components were recleaned and the system produced undoped thick films ($> 75 \mu\text{m}$) with $2 \times 10^{15}/\text{cm}^3$ net carriers. However, thin undoped films gave net electrical carriers of approximately $1 \times 10^{16}/\text{cm}^3$. The reason the thicker films were lower in carriers is because predeposit which forms on the quartz above the substrate acts as a getter for impurities. Hence, the longer the deposition cycle the greater the predeposit and the higher the purity of the deposit. The epi film thus contains a carrier gradient.

The major background impurity has been identified as silicon from an emission spectroscopy analysis of an undoped film approximately $90 \mu\text{m}$ thick. The results of the analysis, given in Table II, shows the silicon concentration is an order of magnitude higher than the measured carriers. This result may be slightly high but it indicates that the major background impurity is derived from the quartz reactor and not from the various feed sources. It has been found in previous work on epitaxial GaP that silicon is also the major impurity and that it is formed primarily from reactions between HCl and the quartz.

So far attempts to drastically reduce the background level by changes in reactor design have been unsuccessful. Additional work along this line will be continued into the next quarter.

C. RESULTS OBTAINED ON THE GROWTH OF HIGH RESISTIVITY GaAs IN RESEARCH SCALE REACTORS

In order to employ d. c. modulation techniques on GaAs waveguides, high resistivity epitaxial layers will be required. In order to achieve layers with the desired $> 10^6 \Omega\text{-cm}$ resistivity it will be necessary to develop a technique for compensating the epitaxial layers.

This work has been initiated in laboratory scale horizontal reactors, in order to minimize developmental costs. Two approaches are being used in the attempt to produce high resistivity VPE layers of GaAs using the laboratory scale reactors, Zn-O doping and Cr doping. In the first approach, light zinc doping should completely compensate the normal background donor impurities and partially compensate deep donors introduced by oxygen doping. In the second approach sufficient chromium, which introduces a deep acceptor level, must be added to over compensate the background donor impurities.

An initial attempt at Zn-O doping was apparently successful. An n/I/n structure was grown consisting of a 2 mil Zn and O doped layer grown on an n-type substrate followed by a 1 mil n-type layer of Te doped GaAs. The leakage current in either forward or reverse direction of diodes (12 x 12 mil chips on ceramic header) fabricated from this sample indicated a resistivity of $> 10^7 \Omega\text{cm}$ for the Zn-O doped insulating layer. Subsequent attempts to grow Zn-O doped layers on large area substrates, however, have resulted in p-type layers with hole concentrations near $10^{17}/\text{cm}^{-3}$. The cause of the unexpectedly high Zn concentrations is under investigation. Some system contamination with zinc and carry-over from prior runs has been observed, but not at such high concentration.

Results of chromium doping experiments to date are inconclusive. Either Cr metal or CrCl_2 have been used as the dopant source, placed in a small boat upstream of the substrates in the hottest zone of furnace. With one chromium source low resistivity p-type layers were obtained, evidently due to a p-type impurity in the chromium. Using a different chromium source in a reactor modified to permit location of the chromium in the GaCl-H_2 stream out of contact with arsenic or deposited GaAs, a single run has produced low mobility, n-type material. Several runs have employed CrCl_2 as the source of Cr dopant. I-V characteristics of diodes fabricated from the resulting material have indicated that high resistivity was not achieved.

An alternative dopant for high resistivity GaAs is Fe which may be more easily incorporated in VPE GaAs, but does not produce as deep an acceptor level as Cr. If attempts to achieve sufficient Cr doping continue unsuccessful, Fe doping will be tried.

D. WAVEGUIDE STRUCTURES SUBMITTED FOR EVALUATION

As described in Section C. the majority of the time spent on the program during this reporting period has been devoted to the growth of large area epitaxial layers with uniform thickness and low net carrier concentrations. In addition, however, eight waveguide structures have been grown and submitted to the Washington University team for evaluation. The characteristics of the structures are summarized in Table III. All of the waveguides had lengths in excess of 1" and in most cases the usable length was ~ 2". The GaAs substrates were between 15 and 20 μm thick, and were mechanically and chemically polished on both sides. The bottom of the substrate was polished in order to allow coupling of light into and out of the waveguide through the substrate as described in Section IV. During the growth of the epitaxial layer the bottom surface was protected by coating it with an SiO_2 film.

E. CONCLUSIONS

- 1) Film thickness uniformity of $\pm 5\%$ can be obtained with GaAs films of approximately 50 μm thick using a rotating flat disk holder.
- 2) A low density of shallow irregular shaped pits are present in thick epitaxial GaAs films. Whether or not these pits present a serious problem has not yet been determined.
- 3) Relatively high background contamination is due to silicon formed by reactions of HCl with quartz.
- 4) High resistivity GaAs epitaxial films have been grown using Zn-O doping. However, suitable layers cannot yet be grown reproducibly, and further exploratory work is required.

TABLE I

Epitaxial GaAs Film Thickness Uniformity

Using a Rotating Disk Holder

Run 5-102		Run 5-134	
<u>Distance</u> <u>mm</u>	<u>Film Thickness</u> <u>μm</u>	<u>Distance</u> <u>mm</u>	<u>Film Thickness</u> <u>μm</u>
0	34.2	0	49.0
5	29.4	5	45.1
10	29.4	10	46.6
15	29.4	15	46.6
20	29.4	20	42.7
25	31.9	22	44.1
28	33.8		

TABLE II

Emission Spectroscopy Analysis of Undoped Epi GaAs

Run No. 5-201

<u>Element</u>	<u>Atoms/cm³</u>
Ai	9×10^{15}
Cr	N. D.
Ge	N. D.
Fe	3×10^{15} (EST.)
Pb	N. D.
Mn	N. D.
Mo	N. D.
Pt	N. D.
Si	1.0×10^{17}
Sn	N. D.
V	N. D.
Zn	N. D.
Sb	N. D.
Ni	N. D.
In	N. D.
Cu	9.0×10^{13}
Mg	3.0×10^{15}
Ti	N. D.
Ag	N. D.

N. D. --- Not Detected

EST. --- Estimated

Measured Net Electrical Carriers = $1.0 \times 10^{16}/\text{cm}^3$

TABLE I

Characteristics of GaAs/GaAs Waveguide Structures

Epitaxial Layer Thickness (μm)	Epitaxial Layer Carrier Concentration (carriers/ cm^3)	Substrate Carrier Concentration (carriers/ cm^3)
29 μm	1.5×10^{16}	1×10^{17}
"	"	6×10^{17}
"	"	1×10^{18}
"	"	4×10^{18}
26 μm	2.7×10^{15}	1×10^{17}
"	"	6×10^{17}
"	"	1×10^{18}
"	"	4×10^{18}

SECTION III

LIQUID PHASE EPITAXY

A. INTRODUCTION

The primary objective of the Liquid Phase Epitaxy (LPE) portion of the program is to grow GaAs/GaAlAs epitaxial structures on GaAs substrates. A series of structures with different layer thicknesses, carrier concentrations, and alloy compositions will be investigated in order to determine an optimum waveguide structure.

The primary goal of LFE work will be to ascertain whether the GaAlAs system offers a significant improvement in performance over that obtained with GaAsP or GaAs devices which can be grown using the more highly developed VPE Technology.

B. EXPERIMENTAL SYSTEMS

1. Radiant Furnace LPE System

This furnace and control system is a Model 5313 Closed-Loop Radiant Heating System made by Research, Inc., Minneapolis, Minn. The furnace is a parabolic clamshell with twelve tungsten infrared heat lamps which provide a ten inch heated length. The furnace is controlled by a Thermac Model 5192 regulation unit and solid state power controller, which is programmed by a Model FGE 5110 Data Trak unit.

The use of a high response, negligible thermal mass furnace offers a fast turn-around time for epitaxial growth. The $\pm 0.1^\circ\text{C}$ temperature control and the continuously variable temperature control from fixed point control up to the quenching rate of the furnace and susceptor results in a unit well suited for the LPE growth of small-area experimental epi-layers.

The susceptor or sliding boat used with this radiant furnace system is shown in Figure 1. The boat has a length of 6 inches and is constructed from POCO graphite. The boat and melt are stationary and the substrate slides under the melt. The top and bottom halves of the boat are held together with graphite pins. The boat will accommodate a $3/4 \times 1-1/4$ inch substrate.

The gas reagent handling system is shown in Figure 2. The layers are grown under a purified hydrogen ambient and helium is substituted when the reactor is opened for product removal. A flow of HCl is used for reactor cleanup, H_2S for n-type doping and AsH_3 for melt saturation.

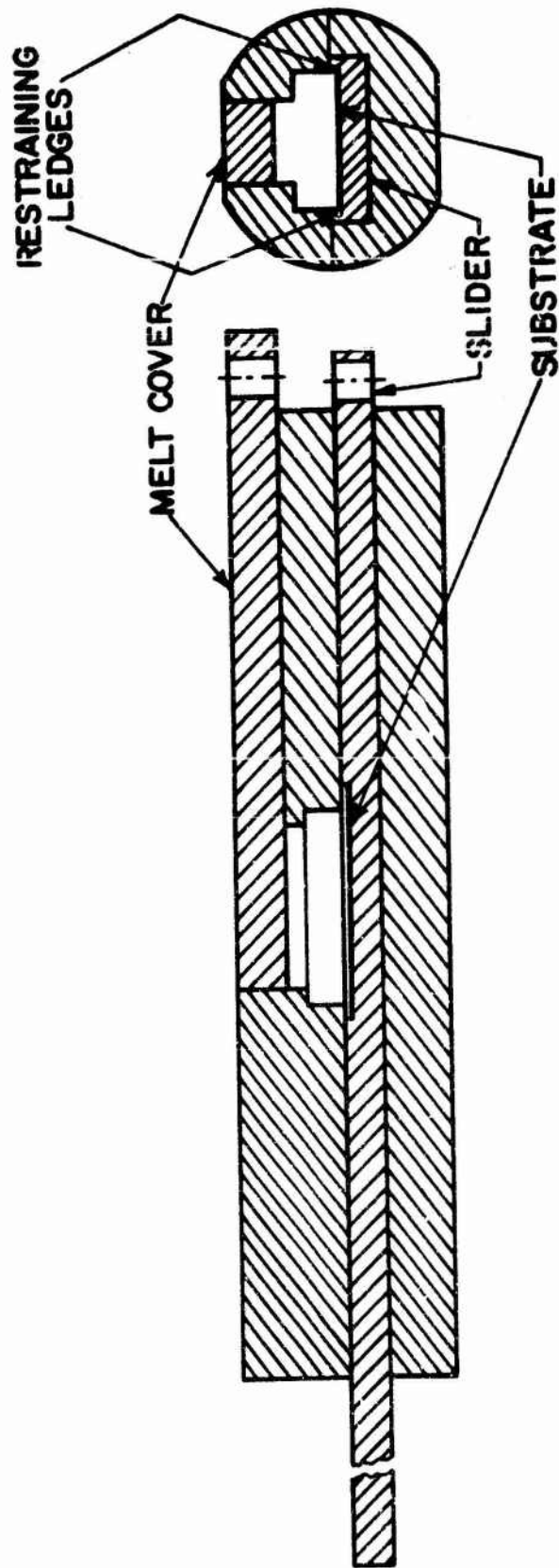


Fig. 1 Research Scale LPE Graphite Boat

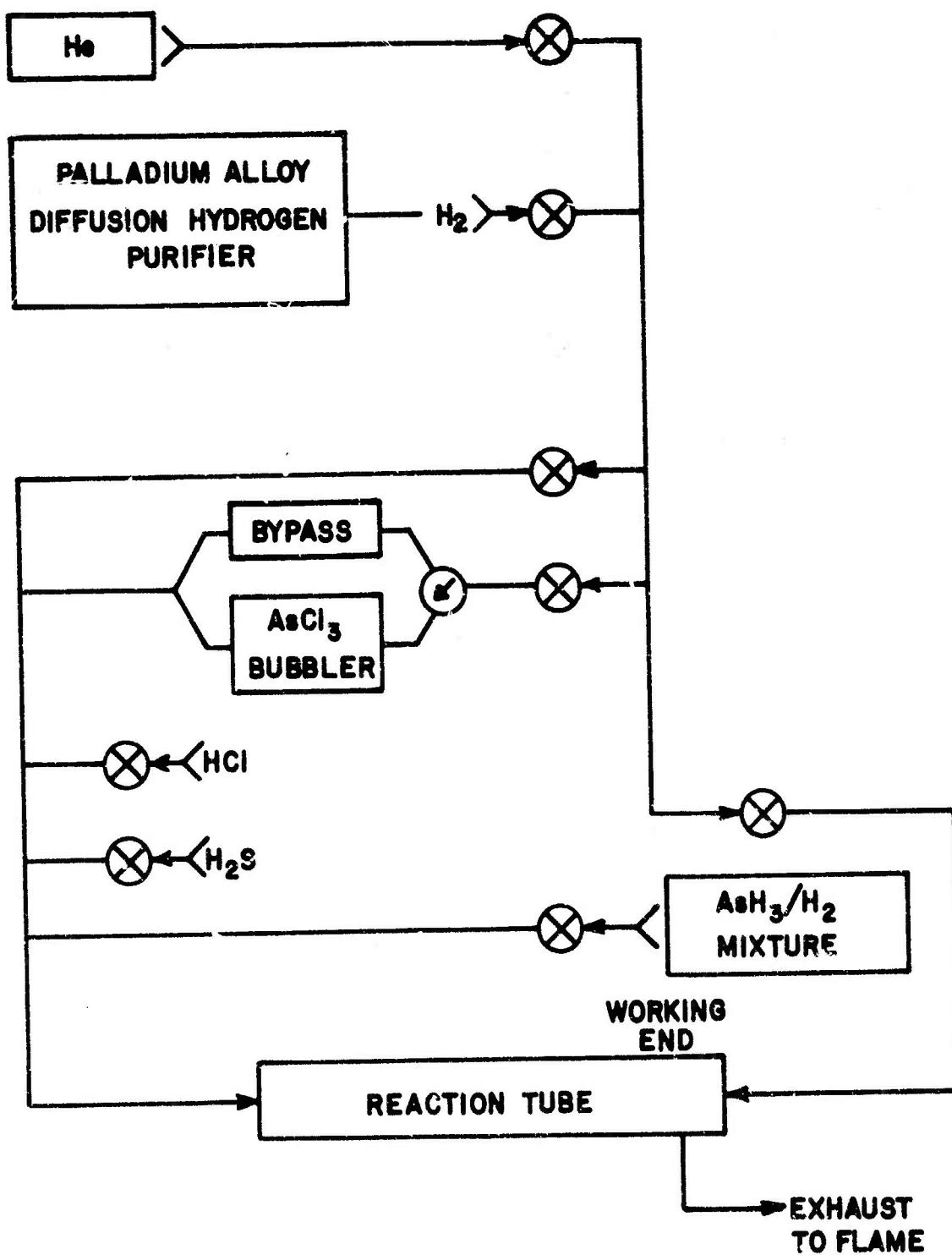


Fig. 2 Schematic of Gas Handling System

2. Resistance Furnace LPE System

This system utilizes a Lancer Diffusion Furnace (Lindberg Hevi-Duty) with a 4-3/4 inch bore and a 53 mm I.D. Quartz reactor tube. The furnace has a 20 inch flat temperature zone to $\pm 0.5^\circ\text{C}$ and can be programmed to cool at a rate of $0.1^\circ\text{C}/\text{min}$ up to the no-current cooling rate of the furnace ($\sim 5^\circ\text{C}/\text{min}$ at 800°C).

A large-area graphite slider-boat was designed and constructed to accommodate the long substrates required for the waveguide program. A schematic drawing of the boat is shown in Figure 3. Since the above furnace is a closed-tube furnace and saturation from the gas phase cannot be observed by opening the furnace, the melt is approximately saturated by the addition of solid GaAs to the Ga and true equilibrium between the liquid and solid phase at the start-of-growth temperature is established by moving the melt (sliding plate 1 and 2) over additional source material. After temperature and compositional equilibrium has been established the melt is moved on top of the substrate for the growth cycle. The boat was designed for a 3/4 x 2 inch substrate, which required the construction of a 12 inch boat.

C. EXPERIMENTAL RESULTS

1. Radiant Furnace System

A series of 28 runs have been made to determine the growth parameters required for the growth of undoped GaAs epi-layers with a uniform layer thickness. The early runs produced layers with a carrier concentration in the high $10^{17}/\text{cc}$ range. All parts of the graphite were then commercially purified (by POCO Graphite, Inc.) and subsequent runs indicated that layers with background carrier levels in the mid $10^{15}/\text{cc}$ could be obtained.

The surface quality and layer thickness uniformity have not been satisfactory for waveguide measurements. Cooling rates in the range of 0.5 to $6.5^\circ\text{C}/\text{min}$ have been investigated; the slower growth rates appear to produce slightly improved surface quality. Starting-growth temperatures have generally been near 775°C , but trial runs up to 930°C have been made without significant changes in surface quality or layer thickness uniformity. Although layers with a thickness variation of only $\pm 10\%$ are often observed over the central area of the wafer, severe edge effects are always present.

In a recent run, a layer of GaAlAs was grown on a GaAs substrate. The surface quality was good, showing only minor stacking fault lines, but the thickness variation was $\pm 20\%$ with the layer becoming thinner toward the edges. It has become apparent that the relatively small mass of the six inch boat plus the short flat temperature zone of the radiant furnace precludes the growth of large area uniform epi layers. The construction of a 12 inch

GRAPHITE SLIDER BOAT (Schematic)

1/2 Scale

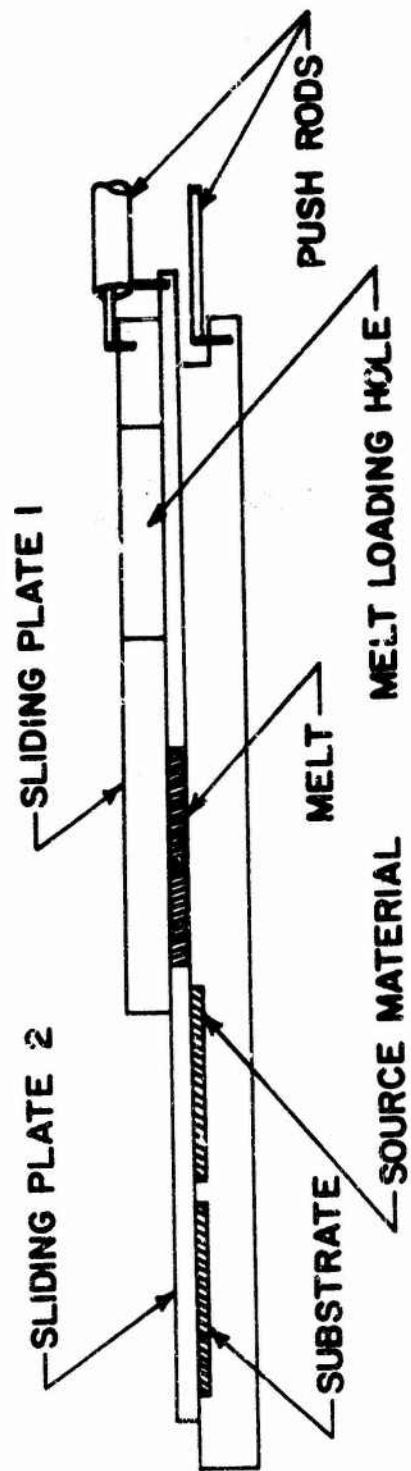


Fig. 3 Schematic Diagram of Graphite Sliding-Boat System

slider-boat has now been completed and the major LPE effort will be shifted to the optimization of growth conditions using this boat in the large resistance furnace.

2. Resistance Furnace System

Several trial runs have been made in the recently constructed 12 inch slider-boat to check its mechanical operation, before subjecting it to a final purification. A short in-house purification using HCl gas at 1000°C has been made. The trial runs indicated that the mechanical operation is satisfactory but the GaAs epi layers had a poor surface quality due to improper wetting of the substrate surface with the melt. This may be due to impurities degassing from the graphite. Schottky barrier (C/V) measurements indicated that the layer had a carrier concentration of $5 \times 10^{15}/\text{cc}$. A graphite purification should lower this level, although the impurities in this system may become limited by the purity of the solid GaAs source material available for the melt.

D. CONCLUSIONS

- 1) The small radiant heat furnace is not suitable for the growth of large area waveguide structures.
- 2) A 12 inch graphite slider-boat has been constructed which is satisfactory from a mechanical point of view, and should exhibit suitable thermal properties for the growth of waveguide structures.

SECTION IV

WAVEGUIDE EVALUATION

A. EXPERIMENTAL MEASUREMENT OF THE WAVEGUIDE ATTENUATION

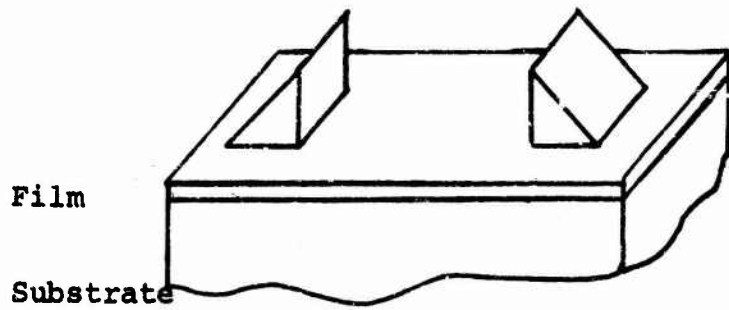
1. Methods of Experimental Measurement

Several schemes have been considered and tried to determine accurately the attenuation rate of the epitaxially grown thin film waveguides. In all these schemes a laser beam is coupled into the waveguide. The power coupled out from the waveguide is measured for various lengths of propagation within the thin film. Assuming that the input and output coupling efficiencies are constant, then the slope of the semi-log plot of output power versus path length yields the attenuation rate of the waveguide. These schemes are illustrated in Figure 4.

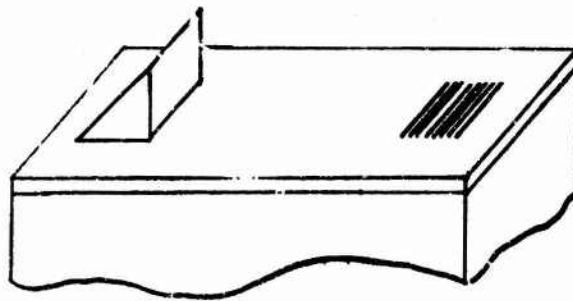
In the first scheme the guided wave is coupled in with a prism and coupled out with a prism. The propagation path length within the film is varied by sliding the output prism back and forth. A second scheme utilizes the prism to couple the light in and a grating to couple out. The propagation path length is varied by sliding the input prism. A third scheme uses a grating coupler for both input and output. The propagation path length can be varied in discrete steps by making several gratings with different distances of separation between the input and the output coupler. Finally, a fourth scheme uses a grating for coupling in and a prism for coupling out.

Both the prism and the grating coupler have been experimentally fabricated and tested with the high resistivity GaAs layer waveguide on a low resistivity GaAs substrate. Over 40% input coupling efficiency and nearly 100% output coupling efficiency were obtained experimentally with the prism coupler. But the grating output coupler only gave a diffraction efficiency of about 10% into the air region. The diffraction efficiency into the substrate is much higher. However, with the low resistivity GaAs substrate, the diffracted beam was heavily attenuated before it emerged from the back surface of the substrate. From our theoretical work (2) we expect the grating efficiency from the substrate side will be quite high and the substrate attenuation much lower when GaAs on GaAsP (or GaAs on GaAlAs) waveguides are used in the future.

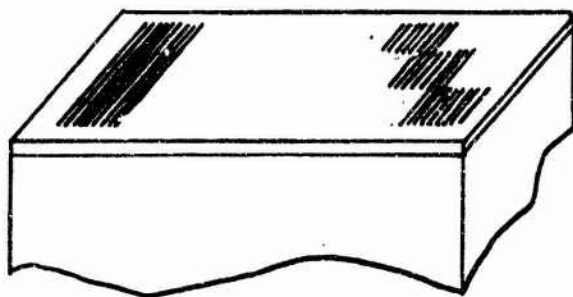
The prism coupler has the advantage that its efficiency is high and it is easily movable. But it has the disadvantage that its coupling efficiency depends upon the flatness and the cleanliness (i. e. the size of the dust particles) of both the epitaxial layer surface and the prism bottom surface. As the prism is moved, the coupling efficiency is not always reproducible. This is particularly true with an input prism coupler. In principle, the output prism coupler efficiency should be much less sensitive to these



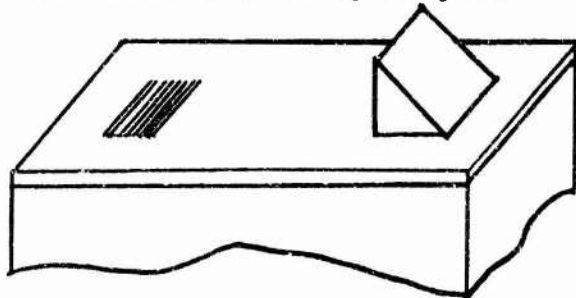
(a) Prism-Prism Coupler



(b) Prism-Grating Coupler



(c) Grating-Grating Coupler



(d) Grating-Prism Coupler

Fig. 4 Schematic Illustration of Attenuation Rate Measurement

variations. The output coupler should have 100% efficiency for a reasonable range of the air gap distances. But in practice we have found that even the output coupler efficiency is not fully reproducible. The grating coupler, on the other hand, gives fully reproducible results once it has been successfully fabricated on the waveguide. However, we do not yet have confidence that the fabrication process for the grating coupler is reproducible.

It is too early to completely discard any of the four schemes; but we have decided that Scheme No. 1 is the best scheme to use at the present time, especially for the evaluation of the high resistivity GaAs film on low resistivity GaAs substrate. The main advantages of Scheme No. 1 are that (a) the input efficiency of a fixed prism coupler is constant; (b) the efficiency of the output prism is less sensitive to fluctuations in air gap separation; (c) high efficiency is achievable; (d) this scheme is adaptable to different waveguides; and (e) the waveguides are reusable in other experiments after this evaluation.

A special fixture was designed and used for the evaluation of all the waveguides according to Scheme No. 1. This fixture is shown in Figures 5 and 6. Figure 7 shows the entire experimental setup including the laser, the chopper, etc. This particular fixture allows us (a) to control the pressure of the prism against the waveguide by controlling the length of the spring; (b) to slide the prisms in and out, back and forth, accurately and very conveniently; (c) to bond the thin sample securely to the holder so that it will not crack under pressure; and (d) to interchange samples easily.

Significant data has already been collected by this scheme, as reported in the following section. However, several difficulties have been encountered which merit discussion. First, the fluctuation of the laser power caused by the thermal drift of the cavity was too large. Therefore, a piezo-electric feedback control was added to our Coherent Radiation Model 42 laser. The schematic diagram of this laser stabilizer is shown in Figure 8. A portion of the actual stabilization equipment used is shown in Figure 7. Second, when the waveguide attenuation is small (e.g. less than 1 db) fluctuations in the efficiency of the output coupler become the limiting factor in our experimental results. Some of this could be caused by dirt or be due to imperfections in the prism or the film. We found that the data is much more reproducible if the prism and the epitaxial layer are cleaned frequently during the experiment. But on occasion, we believe we have also detected the interaction of the two prisms. This might be attributed to the fact that from the transmission line point of view, both prisms produce a mismatch in the transmission line impedance. The net power transmitted to the film under the output prism will depend upon the reflection coefficients created at the edges of the prism and the electrical distance between the two prisms. Since the guide wavelength is about 3 microns and since the distance of separation between the two edges of the prisms was not controlled to this degree of accuracy, the net observed effect

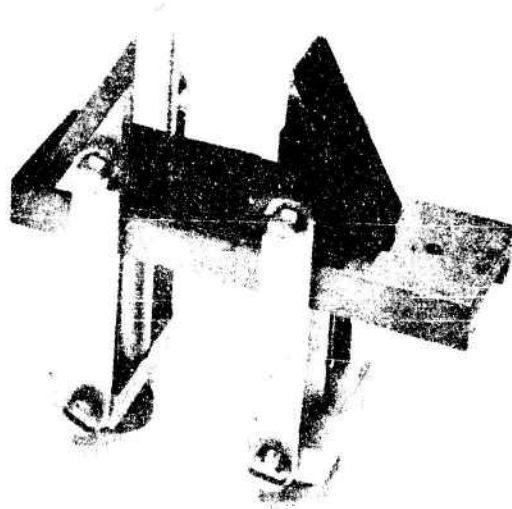
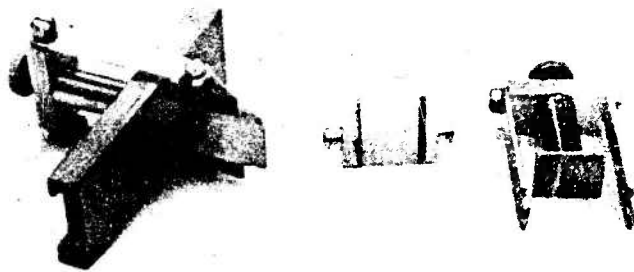


Fig. 5 The Prism-Prism Coupler Assembly

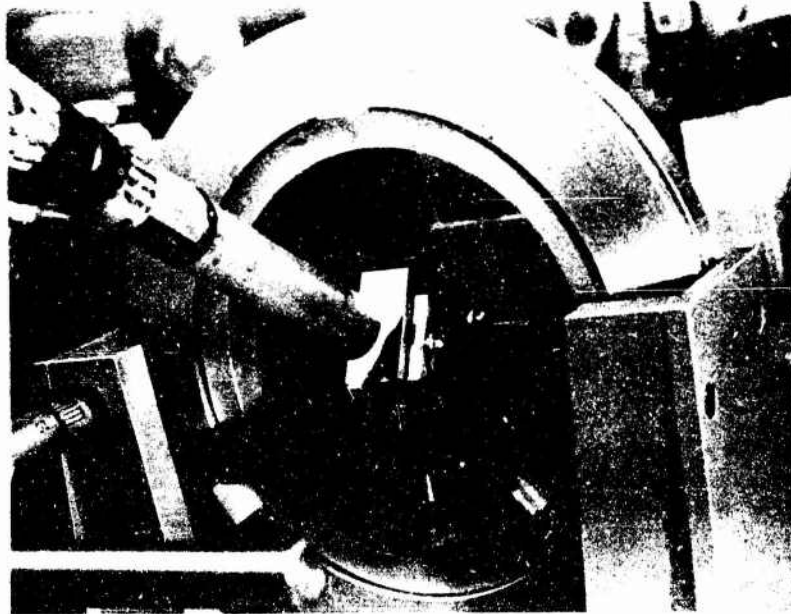


Fig. 6 Measurements of Attenuation Rate by the Prism-Prism Coupler

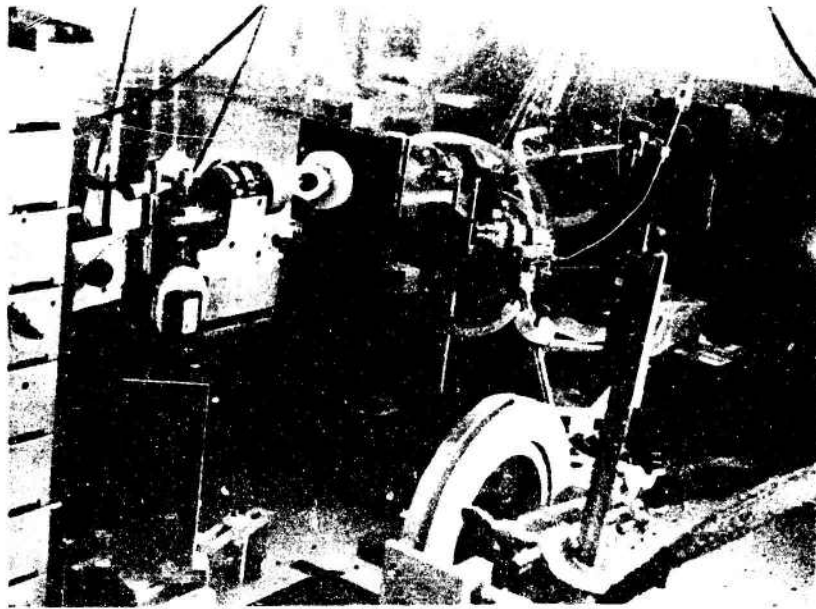


Fig. 7 The Experimental Setup for the Waveguide Evaluation

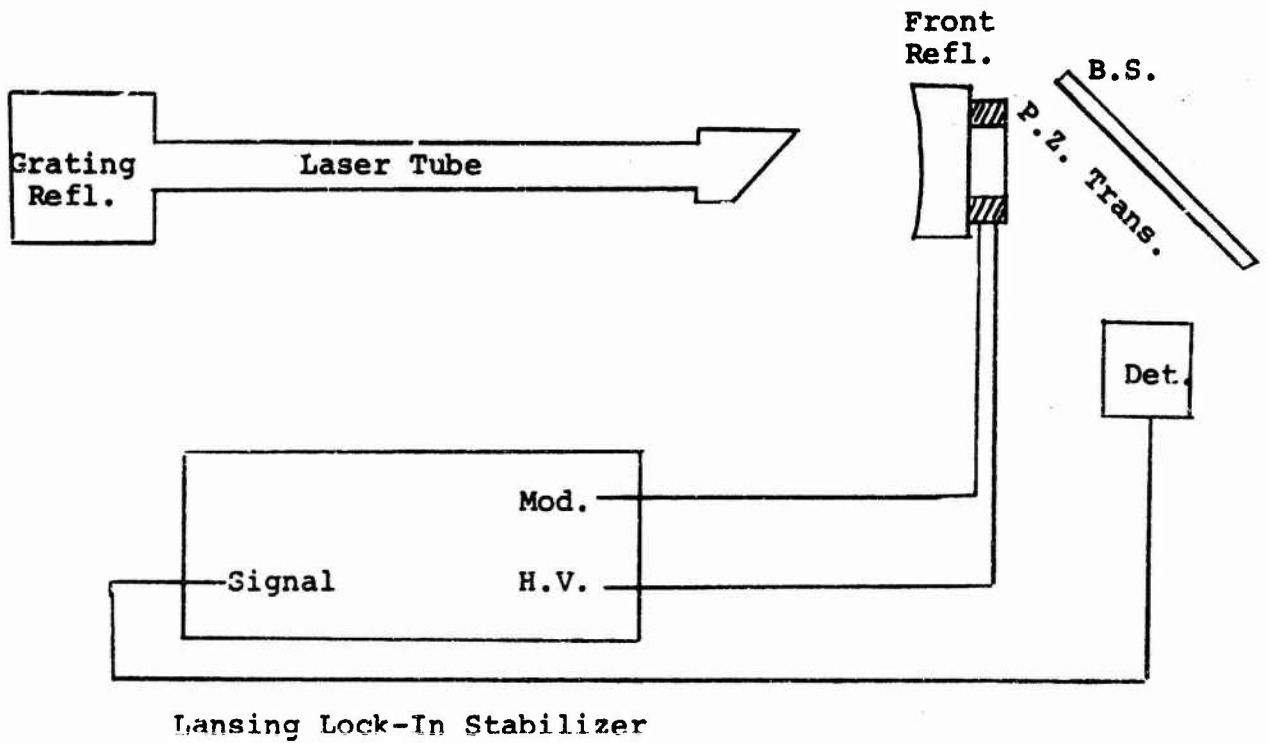


Fig. 8 Schematic Diagram of the CO₂ Laser Stabilizer

is a fluctuation of the detected power coupled out of the prism. Both of these phenomena that led to the fluctuations of the output power are currently being investigated in the project, so that we may establish the limits of accuracy that can be achieved in Scheme No. 1.

2. Experimental Data

Using the experimental method discussed in Section 1, we have gathered attenuation rate measurements data on two waveguides fabricated from material produced in the Monsanto reactor. Figure 9 shows a photograph of a typical wafer and a wafer that has been cut and mounted. The first waveguide has a free carrier concentration of 1.5×10^{16} carrier per c. c. in the film, a film thickness of 29 microns, and a substrate free carrier concentration of 4×10^{18} . The second waveguide has a free carrier concentration of 2.7×10^{15} in the film, a film thickness of 26 microns, and a substrate free carrier concentration of 4×10^{18} . Waveguides with substrate carrier concentrations of $1 \times 10^{17}/\text{cm}^3$, and $1 \times 10^{18}/\text{cm}^3$ have also been grown as indicated in Section II-C. Figures 10 - 13 show the calculated phase velocities (i. e. β_m) of the modes in the waveguides with the various substrate carrier concentrations.

Guided waves were excited in these waveguides by first setting the incident beam at an angle of incidence corresponding approximately to the angle required for phase matching into one of the modes and at a location corresponding approximately to the 90° edge of the prism. The micrometers on the gimble mount and on the translational stage are then used to search for the angles and the positions where a maximum power is coupled out by the prism (and/or is radiated from the edge of the waveguide). The various modes are identified by making the best fit of the observed relative angles of excitation with the calculated angles to satisfy phase matching conditions.

Figure 14 shows the semi-log plot of the measured output power as a function of the path length of the $m=0$ mode and the $m=3$ mode of the waveguide having $N_{\text{film}} = 1.5 \times 10^{16}$ carrier/c. c. and $N_{\text{sub}} = 4 \times 10^{18}$ carrier/c. c. The scatter of the experimental points shows the reproducibility of our output efficiency achieved to date. The average slope of the plot indicated by the solid line shows that the attenuation rate of the $m=0$ mode is 5.6 db/cm and that the attenuation rate of the $m=3$ mode is 13.3 db/cm.

Two conclusions can be drawn from this data:

- (a) The attenuation rate in bulk GaAs, at $10.6 \mu\text{m}$, is related to the carrier concentration by the relationship $\alpha \approx 8 \times 10^{-17} \times N$, (3) where N is the free electron concentration, neglecting a background absorption of 0.02 cm^{-1} which is present even in high resistivity material. (4) Thus, for $N = 1.5 \times 10^{16}$ carriers/ cm^3 the calculated attenuation is 5.2 db/cm. One could not expect the attenuation rate of the guided waves to be much smaller than this. Our measured attenuation rate is reasonable compared to the calculated bulk attenuation rate. In order to improve the waveguide performance, the free carrier concentration of the film must be reduced.

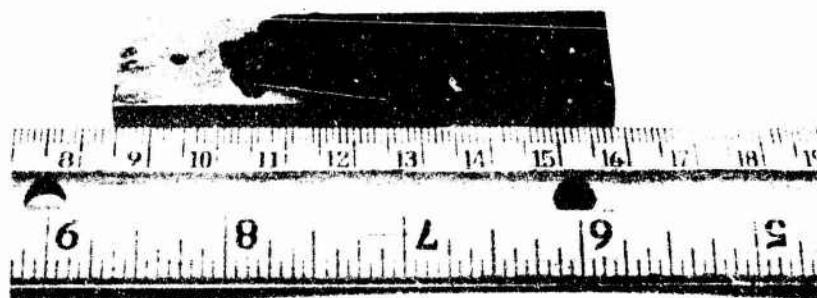
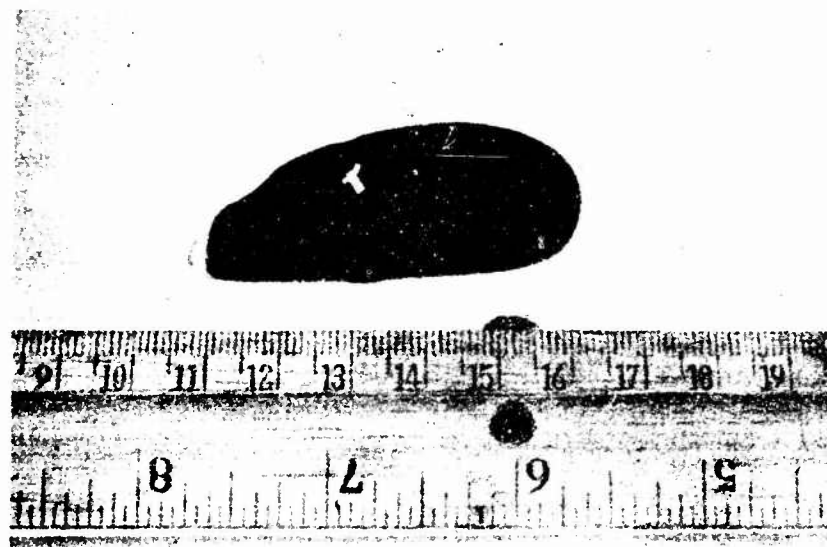


Fig. 9 Photograph of the GaAs Epi-Layer Wafers

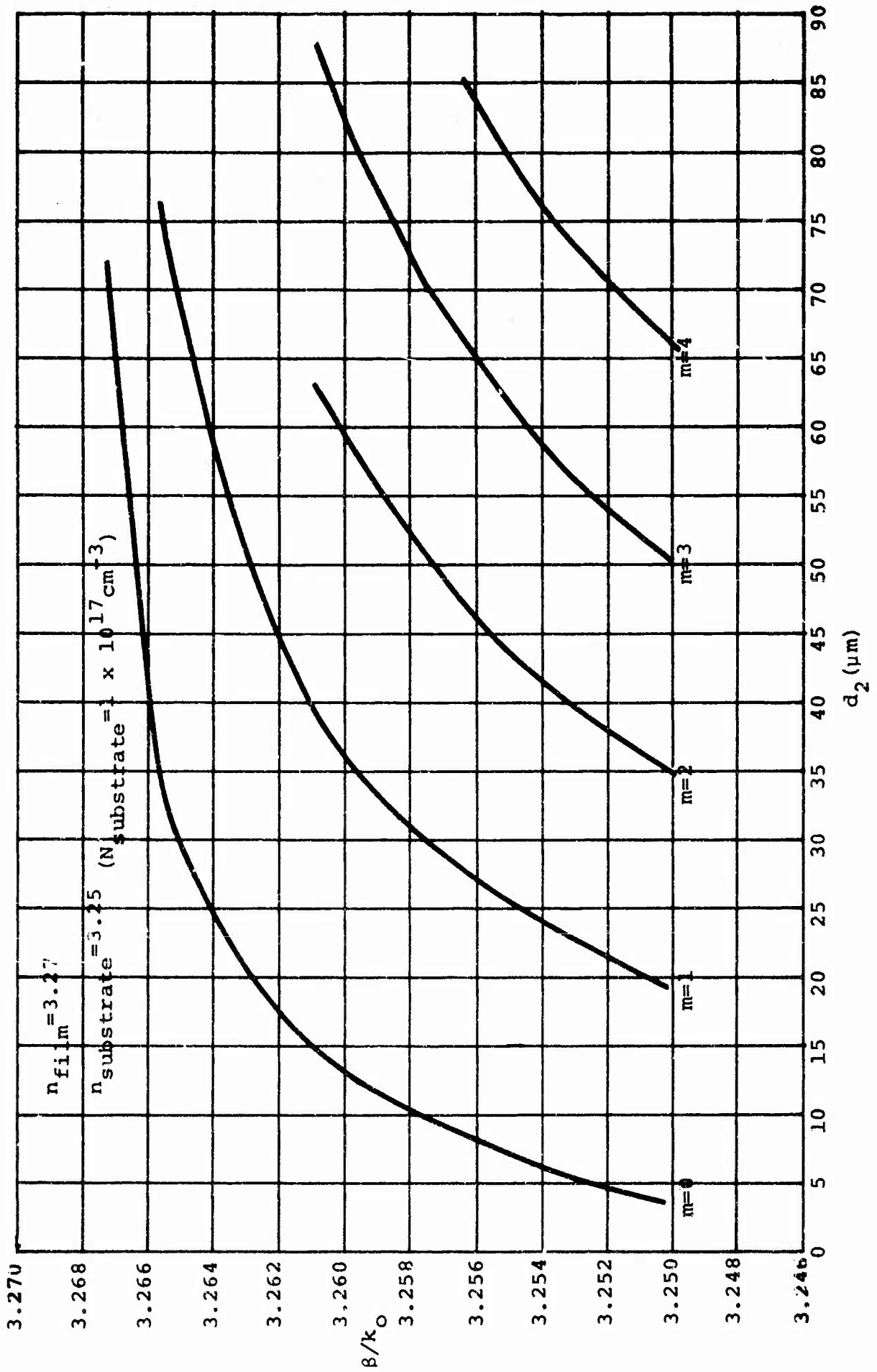


Fig. 10 Calculated Curves for β/k_0 versus Film Thickness for Various Modes

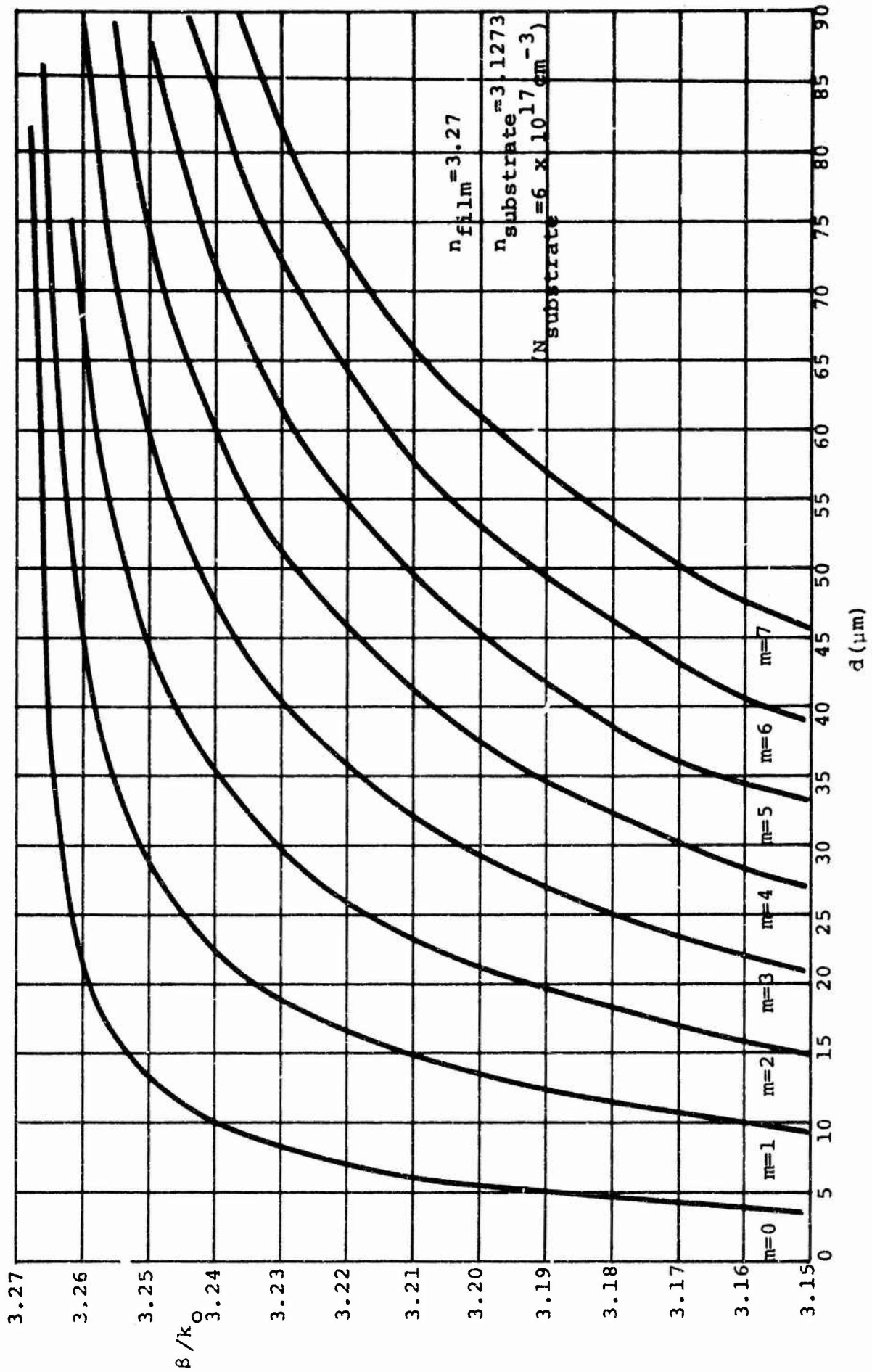


Fig. 11 Calculated Curves for β/k_0 versus Film Thickness for Various Modes

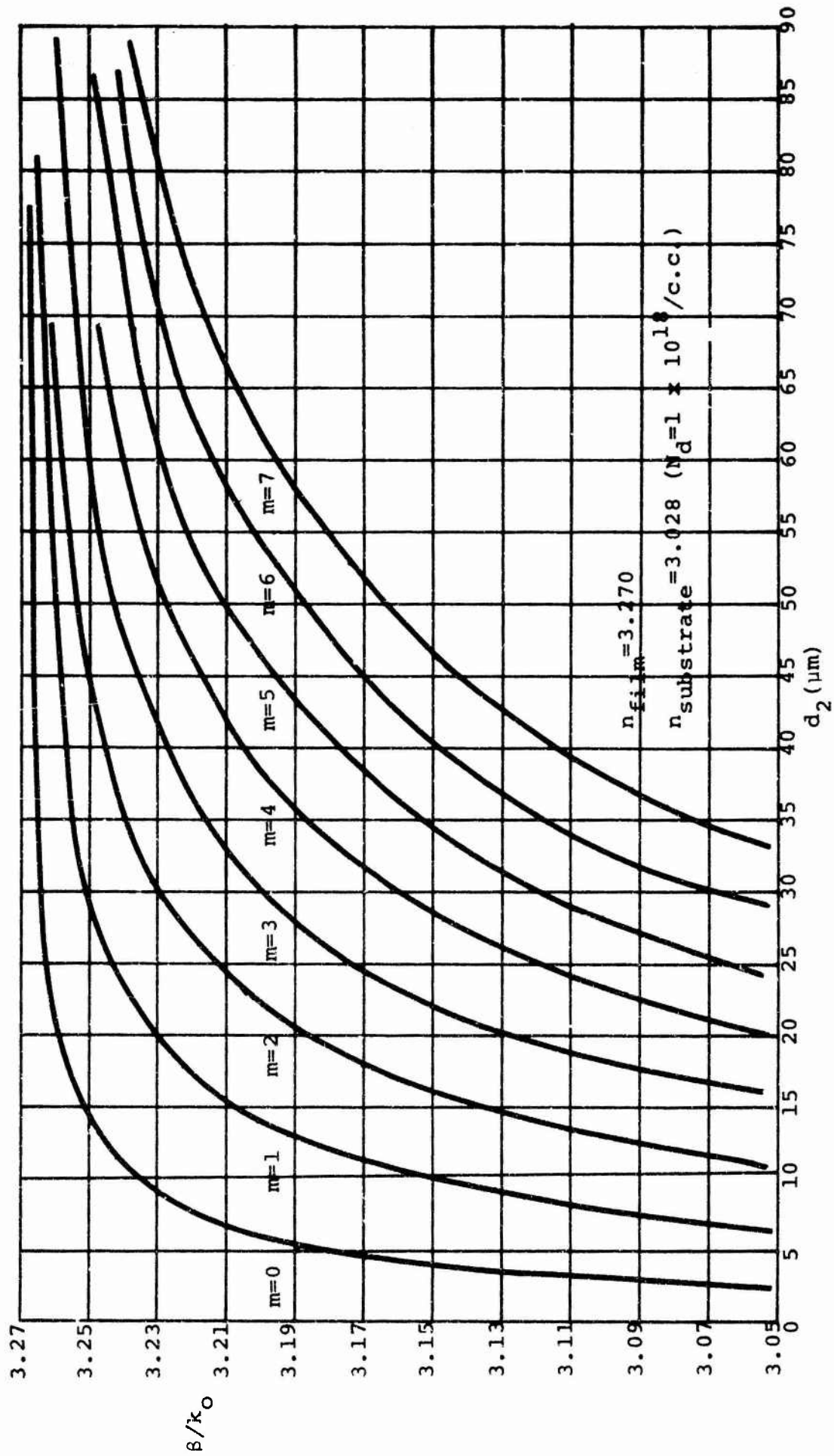


Fig. 12 Calculated Curves for β/k_0 versus Film Thickness for Various Modes

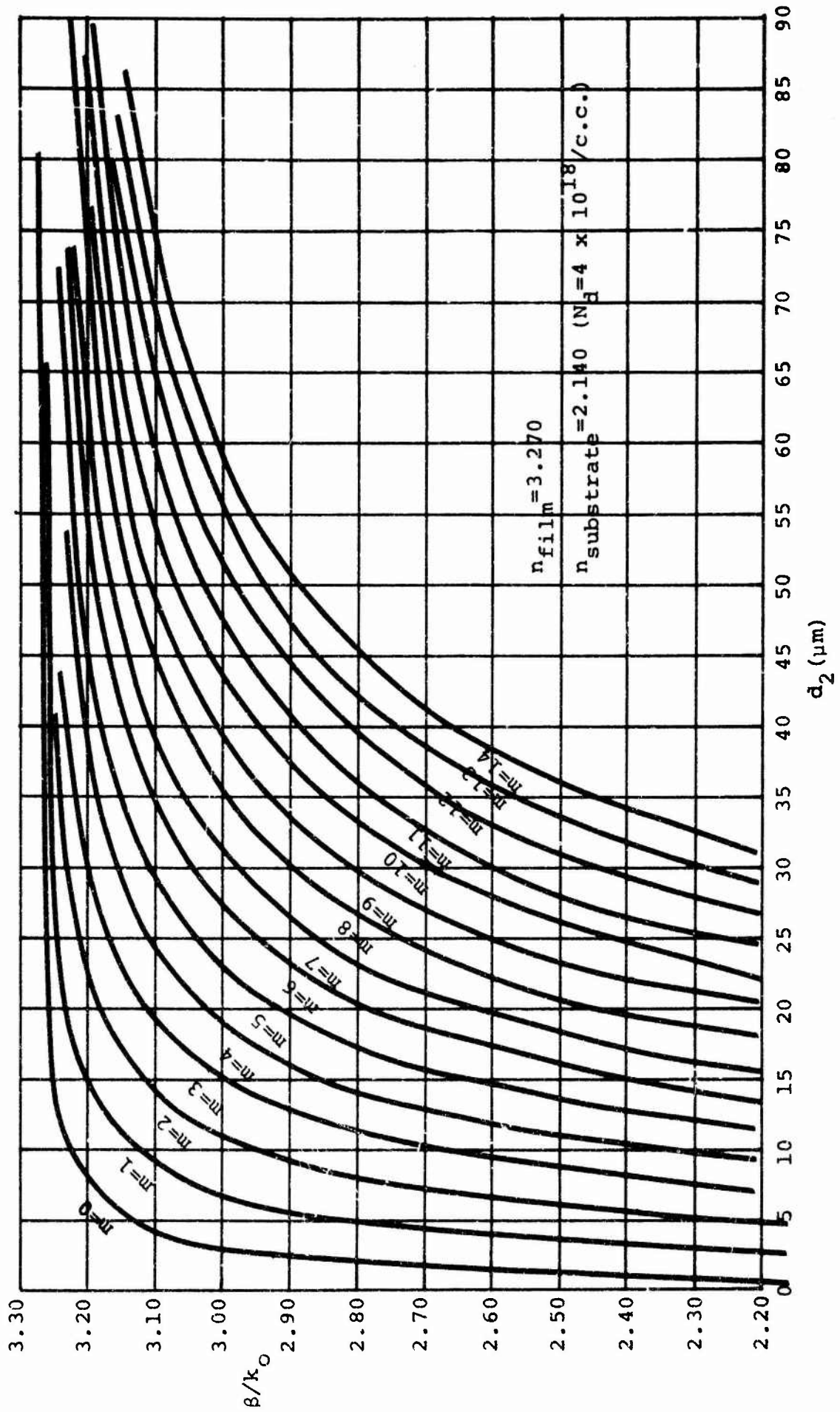


Fig. 13 Calculated Curves for β/k_0 versus Film Thickness for Various Modes

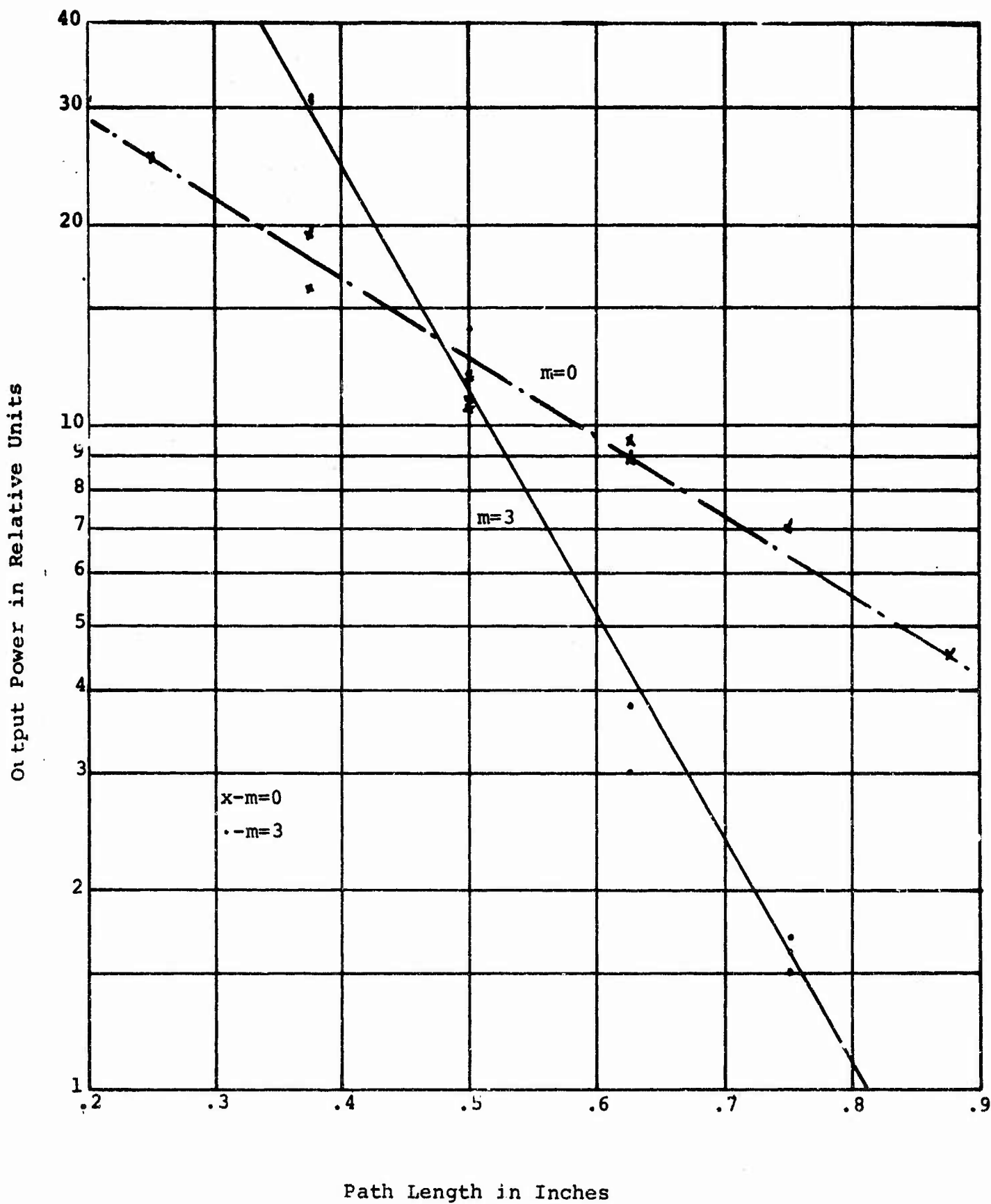


Fig. 14 Relative Output Power as a Function of the Path Length

- (b) The higher order mode has a longer evanescent tail in the substrate. Since the substrate is highly absorbing, one would expect the $m=3$ mode to have a much higher attenuation rate as indicated by our measured result. The significances of this result are: (i) The $m=0$ mode is affected very little by the substrate attenuation, (ii) The attenuation rate of $m > 0$ modes increases very rapidly with decreasing values of β_m because of substrate attenuation.

Semi-log plots of the measured output power V_s path length for the wafer having 26 micron thick film with $N_{\text{film}} = 2.7 \times 10^{15}$ carrier/c.c. and $N_{\text{sub}} = 4 \times 10^{18}$ carrier/c.c. gave the following attenuation rates:

$m = 0$	attenuation rate = 0.7 db/cm
$m = 1$	attenuation rate = 3.4 db/cm
$m = 2$	attenuation rate = 8.2 db/cm
$m = 3$	attenuation rate = 9.6 db/cm

Note that the attenuation rate for the sample with $N_{\text{film}} = 1.5 \times 10^{16}$ is increased by 7.7 db from $m = 0$ mode to $m = 3$ mode. The attenuation rate for the sample with $N_{\text{film}} = 2.7 \times 10^{15}$ is increased by 8.9 db from $m = 0$ mode to $m = 3$ mode.

From the calculated value of the β_m for these two cases, the length of the evanescent tails in the substrate is about the same. One would expect that the increase in attenuation rate should also be the same. Further investigations are planned to determine the significance of this minor difference as additional experimental data is gathered.

The data on the $m=0$ modes for the two samples indicates that the carrier concentration of the epitaxial layer must be reduced further to decrease the attenuation rate of the waveguide. The data showing increasing attenuation with increasing mode number confirmed our suspicion that heavy attenuation caused by the evanescent tail in the substrate will limit the usefulness of this structure as compared to structures of GaAs on GaAsP or GaAlAs.

We have observed some effects on attenuation rate which may have been caused by the imperfections in the epitaxial layer films. However, an insufficient amount of data has been collected to draw any conclusions. Further, it is expected that the data will be much more meaningful when the waveguide attenuation can be reduced to well below 1db/cm. At this moment, we can only say that the experimental results confirm qualitatively our expectation that waveguides at $10.6 \mu\text{m}$ are relatively insensitive to defects in the films.

B. THEORETICAL CALCULATIONS OF THE EFFECT OF SUBSTRATE CONDUCTIVITY ON WAVEGUIDE ATTENUATION

The propagation wave number β_m for the TE_m mode ($m = 0, 1, 2, \dots$) is known to be the $(m + 1)$ th root of the transcendental equation (Ref. 5),

$$\tan \left[\sqrt{\beta^2 - n_2^2 k^2} \cdot t \right] \left[\frac{(n_1^2 k^2 - \beta^2)}{\sqrt{\beta^2 - n_2^2 k^2}} - \sqrt{\beta^2 - k^2} \right] = \sqrt{n_1^2 k^2 - \beta^2} \left(1 + \frac{\sqrt{\beta^2 - k^2}}{\sqrt{\beta^2 - n_2^2 k^2}} \right) \quad (1)$$

Where n_1 = refractive index of the film
 n_2 = refractive index of the substrate
 $k = 2\pi/\lambda$ (λ is the free space wavelength)
 t = thickness of the film

when the substrate has free carrier absorption, n_2 becomes complex.

$$n_2 = n_2^0 - jk_e = \sqrt{\epsilon_r - j \frac{\sigma}{\omega \epsilon_0}} \quad (2)$$

Here ϵ_r is the relative dielectric constant of the substrate at the optical frequency, ϵ_0 is the permittivity of the free space, σ is the conductivity of the substrate, and ω is the angular frequency of the radiation. n_2^0 and the power absorption coefficient α is given as a function of the free carrier concentration in Section IV-A-2. k_e is related to α by

$$k_e = \frac{\alpha \lambda}{4\pi} \quad (3)$$

When n_2 is complex, the roots, β_m , will also be complex

$$\beta_m = \beta_m^0 - j\alpha_m$$

The attenuation rate in db/cm of the mth mode caused by the conductivity of the substrate is related to α_m values (in units of 1/m) by the relationship,

$$\text{attenuation in db/cm of the mth TE mode} = 0.0868 \alpha_m \quad (4)$$

In order to help us to understand the data obtained in Section IV-A-2 we have calculated the values of α_m by means of the transcendental equation under the assumption of

$$\alpha_m << \sqrt{\beta_m^2 - (n_2^0)^2 k^2}. \quad \text{These results are shown in Figure 15.}$$

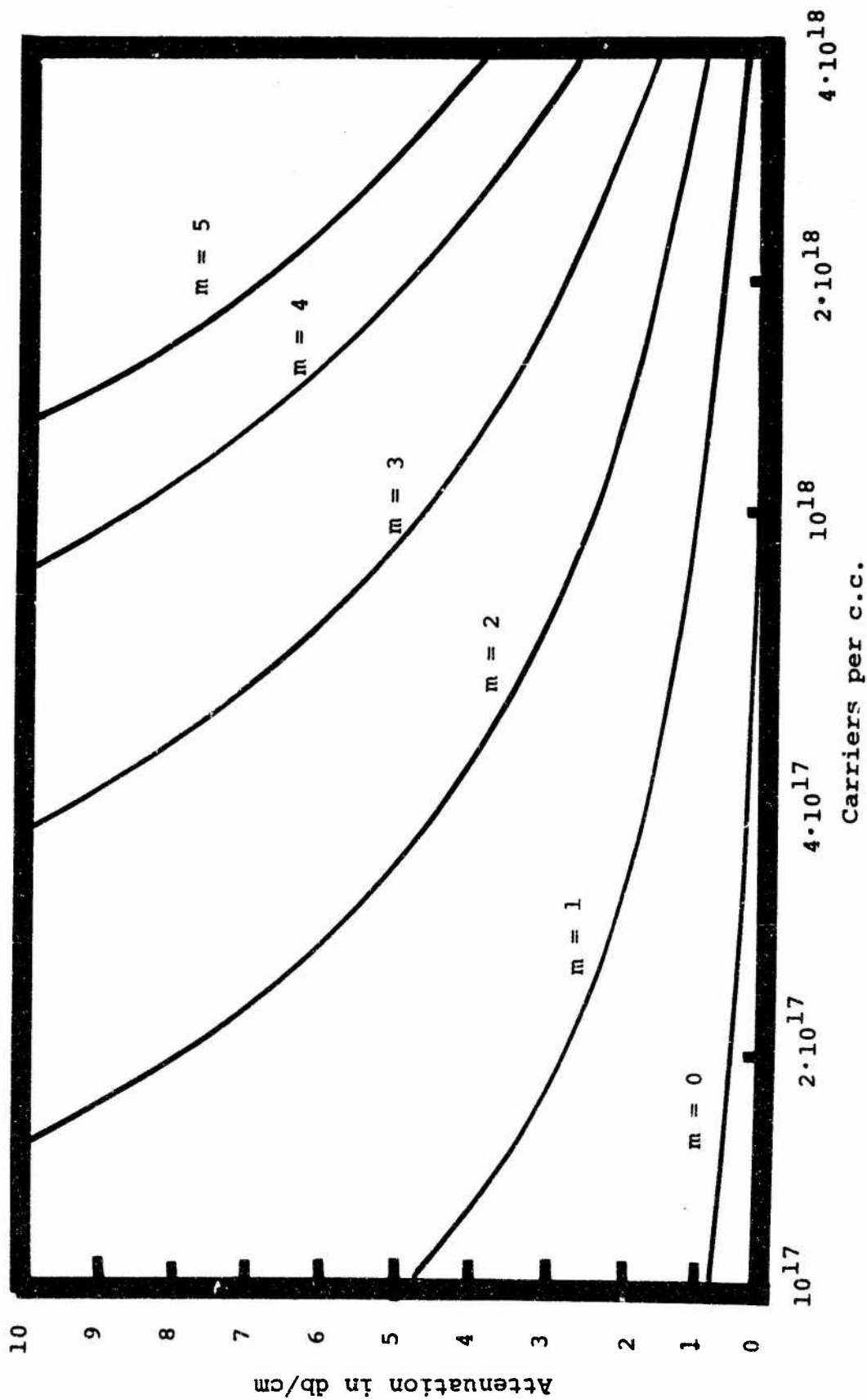


Fig. 15 Calculated Attenuation Rate due to Substrate Absorption, $t = 30$ microns

C. THEORETICAL ANALYSIS OF THE WAVEGUIDES WITH GRADED REFRACTIVE INDEX

In preparation for fabricating waveguide structures in which the refractive index changes gradually from a larger value in the grown film to a smaller value in the substrate we have begun design calculations of mode parameters.

To determine the mode spectrum of a graded-index waveguide we require the phase shift associated with total internal reflection as a function of the index ratio between film and substrate, angle of incidence, and index profile. We assume in all our work that the dielectric constant varies linearly with depth across the transition region of width d . Thus

$$\epsilon(z) = \epsilon_a - (\epsilon_a - \epsilon_s) \frac{z}{d} \quad (5)$$

where ϵ_a is the dielectric constant in the film and ϵ_s is the dielectric constant in the substrate. Since $\epsilon = n^2$, we have

$$n(z) = n_a \sqrt{1 - \left(1 - \frac{n_s^2}{n_a^2}\right) \frac{z}{d}} = n_a \left[1 - 1/2 \left(1 - \frac{n_s^2}{n_a^2}\right) \frac{z}{d}\right] \quad (6)$$

that is to say, when the index difference is small, our assumption is also equivalent to a linear index variation.

To calculate the phase shift, we use the generalized Riccati equation for the reflection coefficient of a varying-index film derived by Walker and Wax (6) but never, to our knowledge, applied to total internal reflection. The equation is

$$\frac{dr}{dz} = 2jkr \sqrt{\epsilon - \epsilon_a \sin^2 \phi_a} + (1-r^2) \frac{d\epsilon}{dz} / 4(\epsilon - \epsilon_a \sin^2 \phi_a) \quad (7)$$

for TE waves and

$$\frac{dr}{dz} = 2jkr \sqrt{\epsilon - \epsilon_a \sin^2 \phi_a} + (1-r^2) \frac{d\epsilon}{dz} (\epsilon - 2\epsilon_a \sin^2 \phi_a) / 4(\epsilon - \epsilon_a \sin^2 \phi_a) \quad (8)$$

for TM waves, for any $\epsilon(z)$. In Eqs. (7) and (8), $k = 2\pi/\lambda$ is the free space wave number of the radiation and ϕ_a is the angle of incidence. These equations must be solved subject to the boundary condition $r = 0$ at $z = d$. The phase of r at $z = 0$ is the phase shift we are seeking. If we use our assumed profile in Eq. (5), the Riccati equation becomes

$$\frac{dr}{d\eta} = jk \sqrt{1-\eta} r - \frac{1-r^2}{4\sqrt{1-\eta}} \quad (\text{TE}) \quad (9)$$

$$\frac{dr}{d\eta} = j\kappa\sqrt{1-\eta} r - \frac{(\sec^2\phi_a + \eta - 2)(1-r^2)}{4(\sec^2\phi_a - \eta)(1-\eta)} \quad (\text{TM}) \quad (10)$$

where we have introduced the notation

$$\eta = \frac{\left(1 - \frac{n_s^2}{n_a^2}\right)}{\cos^2\phi_a} \frac{z}{d} \quad (11)$$

$$\kappa = 2kdn_a \left(\frac{\cos^3\phi_a}{1 - \frac{n_s^2}{n_a^2}} \right) \quad (12)$$

Equations (9) and (10) must be integrated numerically. The chief difficulty of the numerical procedure occurs at $\eta = 1$ where the equations are singular. To eliminate the singularity we use the following procedure: when $\kappa = 0$, Eqs. (9) and (10) are nonlinear but with separable variables, and exact solutions can be obtained (incidentally, this condition corresponds to an abrupt index change, and the exact solutions of course verify the Fresnel phase shifts). By dividing out the exact solutions, we obtain equations which can be solved without further difficulty, and which yield the phase shifts as functions of n_s^2/n_a^2 , d/λ , and ϕ_a .

Programs have been written and debugged and preliminary results have been obtained at present writing; complete results will be available within a few weeks and will be used for designing growth profiles of single and multi-mode graded-index guides.

D. DEVICE EXPERIMENTATION

In anticipation of the availability of various waveguide structures, we have also given extensive considerations to the use of these waveguides for electro-optical modulation.

1. Electro-Optical Modulation in Uniform Thin Film Waveguides

Under the support of NSF Grant No. GD31854, we have made a theoretical comparison of three methods of electro-optical modulation, namely the phase modulation method, the Bragg's diffraction method, and the mode conversion method. From this analysis we have chosen a particular design to carry out the first experiment on electro-optical modulation in this project. Instead of waiting for the better waveguides to be fabricated, we decided it would be advantageous to experiment with one of the existing waveguides and to gain first hand experience in electro-optical modulation immediately. Improvement in the design can be made later, after the initial experimentation.

Figure 16 illustrates the design of the initial experiment. It is a mode conversion modulator. The grating spacing is chosen to satisfy the phase matching conditions of the β_m values between the $m = 0$ and $m = 1$ modes of the waveguide with $t = 29 \mu\text{m}$, $N_{\text{film}} = 1.6 \times 10^{15}$, and $N_{\text{substrate}} = 6 \times 10^{17}$. In order to avoid any discrepancy between the calculated and the actual β_m value, the β_m values were measured experimentally. Subsequently a grating mask of the correct spacing was made. We are presently in the process of fabricating the top grating electrode and the bottom electrode by photolithographic techniques. Initial experimentation on the electro-optical effect using this structure is expected to begin shortly.

2. Experimentation with Two-Dimensional Waveguides

Our analysis of electro-optical modulation also showed that there is no serious limitation in bandwidth caused by the optical characteristic of the modulators. The major limitation will be the power and voltage requirement of the r.f. circuit which is a result of the very low r.f. impedance of the one-dimensional waveguide modulator. The resistive impedance can be raised by using compensated epitaxial layers. This point has already been discussed in Section II-C. The capacitive r.f. impedance can be raised if we use a smaller transverse beam size. However, the minimum transverse beam size is limited by diffraction effects in the horizontal plane of the one-dimensional waveguide. On the other hand, a two-dimensional waveguide can be sputter etched for $10.6 \mu\text{m}$ applications using conventional photolithographic techniques. The width of such a two-dimensional waveguide can easily be $100 \mu\text{m}$ or less, adjusted to fit the optical power handling requirement of the waveguide. If an appropriate metallic electrode is made on top of a two-dimensional waveguide, phase or amplitude modulation similar to that of the one-dimensional waveguide can be achieved. The distinct advantage of the two-dimensional waveguide modulator is that its r.f. impedance is on the order of 50 ohms even at the lower GHz modulation frequency range. In addition, it is well suited for a traveling guided wave modulator. A sketch of a possible two-dimensional waveguide is shown in Figure 17. Of course, the insertion loss that can occur due to the surface scattering losses of the etched waveguide needs to be investigated and optimized before the two-dimensional waveguide can be useful to us. We are convinced that the two-dimensional waveguide modulator will, to a large extent, solve the r.f. drive problem encountered in the one-dimensional waveguide modulator. We propose that during the next six month period a small fraction of the effort be spent fabricating and measuring the attenuation rate of the two-dimensional GaAs waveguides.

E. CONCLUSIONS

1. A reliable method for the measurement of the waveguide attenuation has been developed. The exact limit of the accuracy of this method will be determined during the next period.

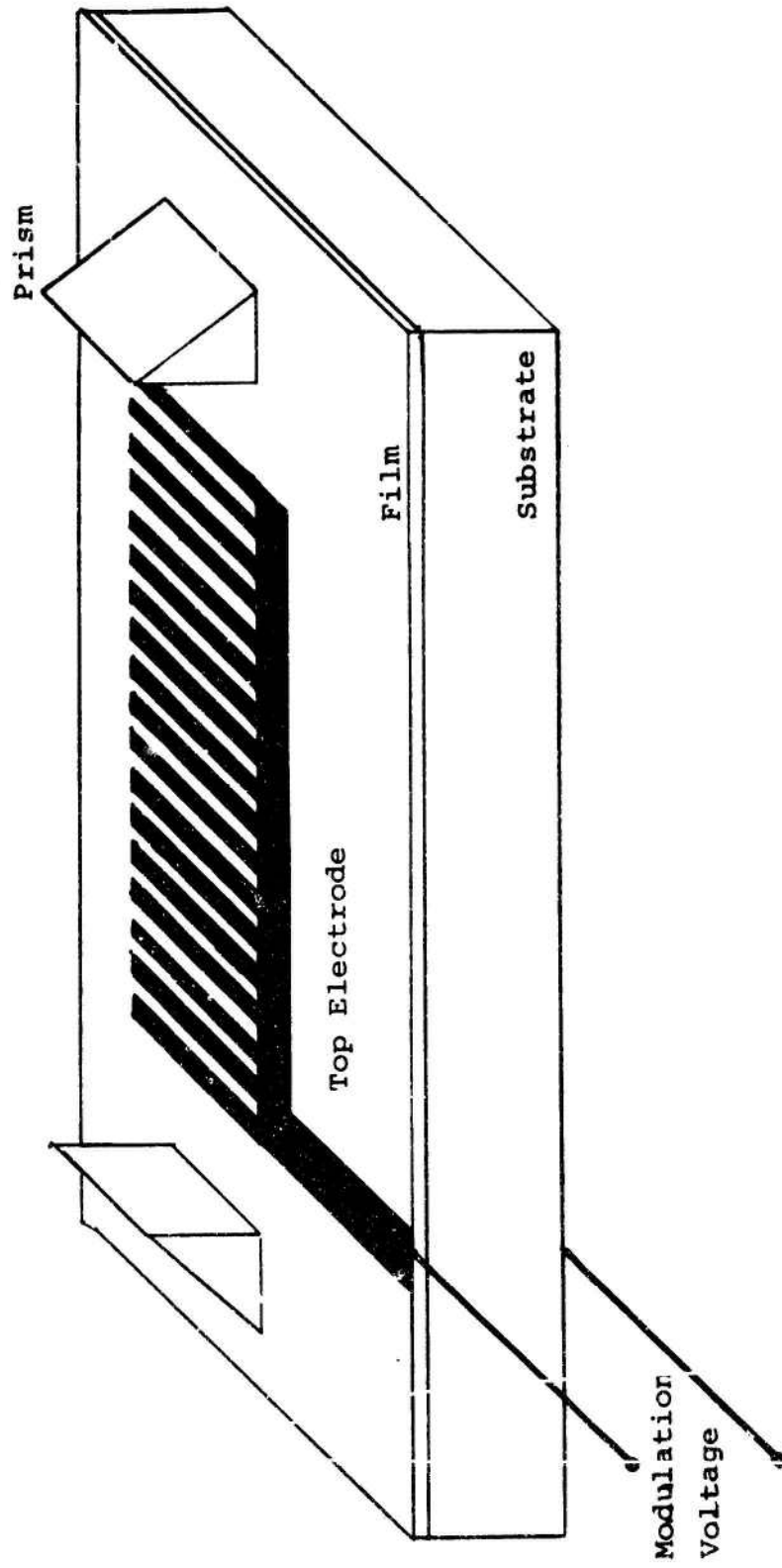


Fig. 16 Schematic Illustration of Grating Electro-Optical Mode Conversion Modulator

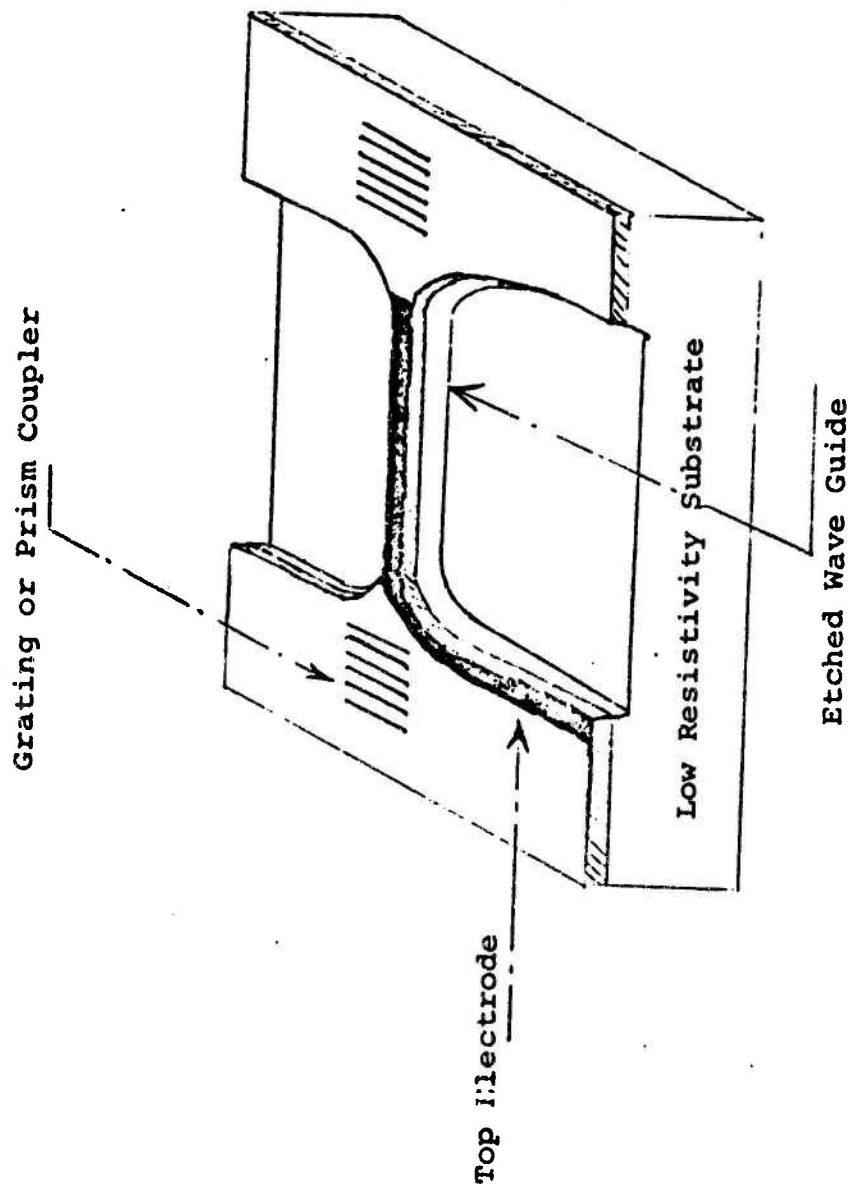


Fig. 17 Two Dimensional Electro-Optical Phase Modulator
 (amplitude modulation can be obtained when the
 electrode is made into grating pattern)

2. From the data collected on the two sets of waveguides fabricated (high resistivity GaAs on low resistivity GaAs structures), we can conclude that: 1) The carrier concentration in the film should be less than $10^{15}/\text{cc}$; 2) The carrier concentration in the substrate will not effect attenuation rate of the $m=0$ mode significantly; and 3) The attenuation rate of the higher order modes increases rapidly as the β value is decreased. The attenuation is caused by the substrate absorption.
3. A computer calculation of the effect of the substrate carrier concentration on the attenuation rate of the waveguide has been carried out. Correlation of this analytical result with experimental data indicates that high resistivity GaAs on low resistivity GaAs waveguide is an effective multi-mode waveguide, for the $m=0$ mode, but not for the higher order modes. While the number of modes increases with an increase of substrate carrier concentration, the attenuation rate for a given mode with a given waveguide thickness is reduced with increase of substrate carrier concentration. This implies that this type of waveguide will be useful for some applications only. We expect the GaAs on GaAsP and GaAs on GaAlAs waveguide will not be limited in the same manner. A complete assessment and trade-off concerning factors such as guide thickness and substrate carrier concentration attenuation versus effectiveness of electro-optical modulation will be made next quarter.
4. An analysis of a waveguide with a graded refractive index has been made in preparation for the experimental fabrication of such waveguide later.
5. The gradient electro-optical modulation experiment has been designed. The initial experiment will be carried out during the next period.

SECTION V

WORK FOR NEXT PERIOD

During the next six months of the project the following tasks will be undertaken:

A. VAPOR PHASE EPITAXY

1. Continue work on reducing background carrier concentration.
2. Achieve reproducible growth of compensated high resistivity GaAs epitaxial films.
3. Grow GaAsP/GaAs and GaAsP/GaAs/GaAsP epitaxial structures with abrupt changes in alloy composition.

B. LIQUID PHASE EPITAXY

1. Additional runs will be made to verify the proper mechanical operation of the 12 inch boat.
2. The graphite boat will be commercially purified.
3. Further work will be carried out to improve the surface quality, reduce the background carrier concentration, and improve the layer thickness uniformity on both GaAs and GaAlAs.
4. An initial series of GaAs/GaAlAs structures will be grown and submitted for evaluation.

C. WAVEGUIDE EVALUATION

1. (a) Complete the data collection of the two sets of wafers already fabricated.
(b) Correlation of the measured data with calculations to assess the trade-offs in the design of GaAs on low resistivity GaAs waveguide. The relevant factors are: guide thickness, substrate conductivity, attenuation rate, effectiveness in electro-optical modulation.
2. Experimentation with E-0 Modulation.
3. Determination of the limitation on the accuracy achievable in measurement Scheme No. 1.
4. Measurement of GaAs on GaAsP waveguides as they become available.
5. Numerical evaluation of the graded index waveguides.

REFERENCES

1. R. A. Ruehrwein, "Manufacturing Methods for Epitaxially Growing GaAs-GaP Single Crystal Alloys," Tech. Rpt. AFML-TR-68-319, Oct. 1968.
2. K. Ogawa, W. S. C. Chang, B. L. Sopori, and F. J. Rosenbaum, "A Theoretical Analysis of Etched Grating Couplers for Integrated Optics," to be published in J.Q.E., Jan. (1973).
3. W. G. Spitzer and J. M. Whelan, Phys. Rev. 114, 59 (1959).
4. R. Weil, J. Appl. Phys. 40, 2857 (1969).
5. P. K. Tien, "Light Waves in Thin Films and Integrated Optics," Appl. Opt., 10, p. 2395 (1971).
6. L. R. Walker and N. Wax, Journal of Appl. Phys., 17, p. 1043 (1946).